Mine Water and the Environment (2022) 41:252–264
https://doi.org/10.1007/s10230-021-00802-1

TECHNICAL ARTICLE

Evaluation of a Superabsorbent Polymer for Plugging Karst Pipe Type Water Inrushes

Chenyang Ma[1] · Shucai Li[1,2] · Rentai Liu[1] · Yan Pei[1] · Chunyu Zhang[1] · Yankai Liu[1] · Fei Xu[3] · Xiao Feng[4] · Mengjun Chen[2]

Received: 11 February 2021 / Accepted: 28 July 2021 / Published online: 4 August 2021

Abstract

In this study, experimentally simulated ultra-rapid and super-large water inrushes was plugged effectively using superabsorbent polymers (SAPs). The SAPs are mainly composed of sodium polyacrylate and possess a core–shell structure at the micro-level, as described through multiple characterization methods. Swelling and flow experiments in a purpose-built apparatus revealed that the SAP can absorb ≈ 300 times more water than its own weight and displays an excellent water retention capacity. Most importantly, when evaluated in a visual model test, the SAP effectively plugged gushing water with high water pressure and a large and/or rapid flow rate; furthermore, the plugging time can be adjusted. Through the experiments, we delineated the plugging mechanism. These research results have important scientific significance and engineering value for reducing and controlling the occurrence of water inrush disasters in karst areas.

Keywords Grouting material · Model test · Karst pipeline · Water inrush control · Water absorbent

Introduction

In karst areas, the construction of tunnels and underground mines are vulnerable to geological disasters (Fan et al. 2018; Ma et al. 2018, 2019a, b; Wang, et al. 2018a, b, c). As listed in Table 1, karst water inrush disasters often occur during underground construction, hinder excavation, and consumes substantial manpower, material resources, and equipment. In serious cases, the foundation or tunnel collapses, and the project fails. In addition, continuous underground water discharge in mines can cause secondary disasters, such as surface collapse, farmland damage, and water source depletion, as well as other issues (Li et al. 2018; Ma et al. 2020).

Grouting is one of the most commonly used methods to manage water inrushes from unfavourable geological bodies. By injecting cement grouting materials into the rock mass, the physical and mechanical properties can be improved to conform to the engineering stability and waterproofing requirements. Numerous studies on grouting materials are available. Ultrafine cement, polyurethane, and cement–water glass are the most often used, and have been thoroughly examined for repairing fine early cracks, strengthening loose or broken structures (i.e. roadways, bridges, and coal mines), and reinforcing dynamic water-rich areas (only for relatively low water flow rates) (Cao et al. 2018; Cui et al. 2019; Duan and Li 2012; Shamsuddoha, et al. 2018; Wang et al. 2018a, b, c; Yuan, et al. 2020). Many experts and scholars have also worked on dynamic water grouting. Wang et al. (2018a, b, c) studied the plugging mechanism of glass fibre cement paste for dynamic water grouting, which effectively improved water inrush situations. Based on different geological conditions, Cui et al. (2017) developed two new cement-based grouting materials (awg-1 and awg-2) that exhibited a strong anti-washout capacity and rapid setting time. Zhang et al. (2018a, b) proposed a new grouting material (HCBGM) to

✉ Mengjun Chen
mjun@sdu.edu.cn

1 Geotechnical and Structural Engineering Research Center, Shandong University, Jinan 250061, Shandong, People's Republic of China

2 School of Qilu Transportation, Shandong University, Jinan 250002, Shandong, People's Republic of China

3 Structural Health Monitoring and Control Institute, Shijiazhuang Tiedao University, Shijiazhuang 050043, Hebei, China

4 School of Transportation Engineering, Shandong Jianzhu University, Jinan 250101, Shandong, China

Table 1 Examples of karst water gushing disasters

Case No	Project Name	Location	Time	Largest inflow (m^3/d)	Consequence
1	Limestone mining	Pingnan, Guangxi Province, China	2018.06	326,000	Project stagnation and fish pond drying up
2	Metal mining	Yifeng, Jiangxi Province, China	2013.08	76,900	Mine collapse, project stagnation, environmental disruption
3	Tunnel construction	Lichuan, Hubei Province, China	2009.12	12,000	Tunnel collapse, surface collapse, and house cracks
4	Hydropower station	Fuyuan, Yunnan Province, China	2017.03	518,000	Dam collapse, land inundation
5	Highway tunnel construction	Shapingba District, Chongqing, China	2003.01	53,000	Surface river irrigation, casualties
6	Railway tunnel construction	Badong, Hubei Province, China	2004.12	50,000	Tunnel collapse, casualties, and major property losses

fill karst caverns when there is flowing underground water prior to shield tunnel construction. However, these grouting materials are all controlled by chemical reactions that are significantly affected by environmental factors, and the grouting materials can easily be eroded and diluted, resulting in inadequate reactions or reaction termination, and unsatisfactory water inrush resolution. Based on this, a new type of expansion material was sought for water inrush treatment.

Super absorbent polymers (SAPs) are new functional polymer gels that can absorb water dozen or even hundreds of times its own weight. SAPs are widely used in different fields due to their unique water absorption and retention properties. In oil exploitation, excessive water production increases oil production costs and limits oil recovery efficiency (Jia et al. 2010; Sun et al. 2019; Yuan et al. 2014). SAP plugging agents have been broadly used to address these issues, including in situ polymer-based gels, preformed particle gels, and microgels (Abdulbaki et al. 2014; Chen et al. 2018; Liu, et al. 2016; Yao et al. 2017; Zhu et al. 2017). In addition, SAPs are also used in agriculture to improve crop survival and yield (Guo et al. 2005; Ni et al. 2012; Wu et al. 2007). However, the use of SAPs has never been reported for the treatment of water inrush.

Inspired by the above research, we performed the following investigations. A type of SAP that possesses a superabsorbent capacity, is non-toxic, and has a good water retention capacity was synthesized. Fourier transform infrared spectroscopy (FTIR) shows that the SAP synthesized by this method contains many hydrophilic groups, which can conform to the swelling requirements. Thermogravimetric (TGA) test results show that the synthesized SAP has good thermal stability and environmental applicability. A visualization simulation device of water inrush in the karst pipeline was designed and assembled so that the migration process of the polymer and plugging mechanism in the karst pipeline could be delineated.

Experimental Methodology

Materials

The materials used were analytical grade acrylic acid (≥ 98.0%), 2,2'-Azobis (2-methylpropionamidine) dihydrochloride (99%), pentaerythritol triallyl ether (≥ 98.5%), chlorophyllin copper complex sodium salt (≥ 97.5%), hydrogen peroxide solution, ferrous sulphate (FeSO4, > 99.7%), and sodium hydroxide (H_2O_2). Unless otherwise specified, deionized water (DI water) with a resistivity of 18.25 MΩ·cm obtained from a water purification system was used to prepare the solutions, and the synthesis procedures were performed at a low temperature (5 ± 1 °C).

Synthesis of the SAP

The SAP was synthesized via bulk radical polymerization. The material quantities used for SAP preparation are listed in Table 2. The synthetic SAP fabrication route is shown in Scheme 1 and the detailed composition method is listed in the supporting information. All SAPs were stored in a desiccator under vacuum until use.

Characterization

Scanning electron microscopy (SEM) images of the swollen SAP structures were taken of samples prepared using the following method. After swelling in DI water for 24 h, the hydrogels were carefully cut, frozen at – 70 °C (FD-A10N freeze dryer), and then freeze-dried under vacuum until the water was sublimated. SEM images of the SAP before and after swelling were obtained using a Hitachi S4800 SEM (Hitachi High-Technologies Co. Ltd., Japan) with a potential of 1000 kV without vapor deposition on the sample surface.

Table 2 Materials, grade, mass fraction, solvent, and quantities for SAP manufacture

Materials	Additive proportion (%)	Details/Description		
		Grade	Mass fraction	Solvent
Acrylic acid (AA)	51.27	≥98.0%	60 wt%	DI water
NaOH	45.64	>99.5%	30 wt%	DI water
Pentaerythritol triallyl ether	1.02	≥98.5%	10 wt%	60 wt% acrylic solution
2,2'-azobis(2-methylpropionamidine) dihydrochloride	0.95	>99%	2 wt%	DI water
Chlorophyllin Cu complex Na salt	0.97	>97.5%	–	–
Ferrous sulphate	0.063	>99.7%	10 wt%	DI water
Hydrogen peroxide solution	0.085	–	10 wt%	DI water

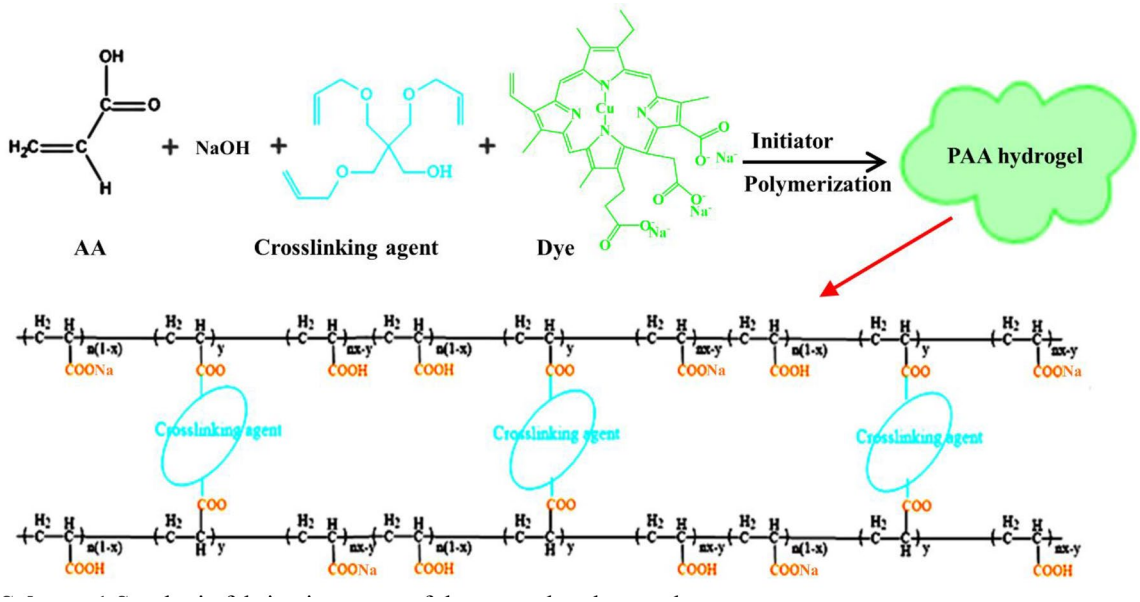

Scheme 1 Synthetic fabrication route of the superabsorbent polymers

The FTIR spectra of the SAPs were measured using a Nicolet model iS10 spectrometer. FTIR spectra were recorded after manually grinding the sample into a powder and mixing it well with KBr. The mixture was compressed into a transparent disk and scanned from 4,000 to 500 cm^{-1} using an average of 16 scans, with a resolution of 1 cm^{-1}. The TGA imaging was conducted by an SDT Q600 V20.9 Build 20 to analyse the thermal stability of the materials in an N2 atmosphere over a temperature range from 10 °C to 700 °C, increasing at a rate of 10 °C/min. The specific surface area of the SAP was determined using an ASAP2460 automatic surface area and porosity analyser provided by Jinan Runzhi Technology Co., Ltd., China. A 0.1 g sample was degassed at 100 °C for 24 h. Subsequently, liquid nitrogen was used as an adsorbent to measure its adsorption capacity at 77 K under different pressures. The adsorption isotherm curve was drawn, and the pore size distribution and specific surface area were calculated. Further characterization analyses were performed using x-ray diffraction (XRD) and Brunauer–Emmett–Teller (BET) surface area analysis techniques, which are described in the Supplemental Information that accompanies the on-line version of this paper.

Water Absorption and Retention of SAP

Water Absorption

The swelling ratio is a key indicator of the water absorption capacity. To measure the swelling ratio of SAPs with different particle sizes in ionic solutions, the synthesized particles were screened. A tea bag (a 400-mesh nylon screen) containing preweighed dry samples was immersed entirely in brine water

and removed every 10 s, followed by the removal of excess surface water using filter paper. The swelling ratio, Sw, was calculated using Eq. 1:

$$S_{\mathrm{w}}(g/\mathrm{g}) = \frac{M_n - M_0}{M_0} \quad (1)$$

where M_0 and M_n are the polymer quantities before and after water absorption for the n^{th} time, respectively.

Water Retention in Natural Conditions

To understand SAP water retention, retention indicators were tested in the laboratory. Prior to the experiment, a certain quantity of SAP was immersed in distilled water at room temperature (20 ± 1 °C). After the swelling equilibrium, residual water on the hydrogel surface of the SAP was wiped off, and W3 (surface dry state) was weighed. The weight of the residual mass was recorded (W4) every five days at ambient temperature (18–26 °C, 30% humidity). The water retention rate under natural conditions is given as Eq. 2:

$$R_2(\%) = \frac{W_3}{W_4} \times 100\% \quad (2)$$

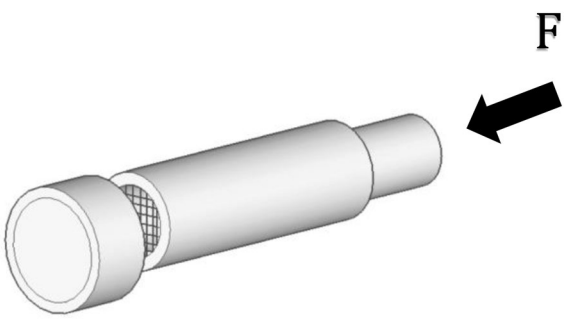

Diagram 1 Schematic diagram of the water retention under the pressure test device

Water Retention Under Pressure

Water retention under pressure, another important indicator for evaluating inrush water plugging capacity, was evaluated with the following experiment. The SAP was immersed in water until the swelling equilibrium was reached; then, the SAP was weighed (marked as W_6 g). Next, the swelling SAP was placed into a measurement device (Diagram 1), composed of a plexiglass bucket (diameter 40 mm, height 30 cm) with pistons; the device was designed to test the SAP's water retention under pressure. The residual mass (W_7 g) was recorded after pressure (0–0.3 MPa) had been applied for 1 min; the water retention under pressure was calculated as Eq. 3:

$$R_3(\%) = \frac{W_7}{W_6} \times 100\% \quad (3)$$

Water Inrush Simulation of a Karst Pipe

A transparent water inrush simulation device for karst pipe flow was assembled in the laboratory to prove the water inrush plugging ability of the SAP slurry. As shown in Diagram 2, this device included five parts: a constant-pressure water supply system, a chemical slurry injection device, karst water inrush pipeline, data acquisition and processing system, and gel collection container. The length and diameter of the visible pipe were 20 m and 40 mm, respectively, and it could be disassembled and connected by a flange. The experimental procedures were as follows: (1) the slurry was configured according to certain proportions and placed into the chemical slurry injection device; (2) the water supply system was opened to provide stable flow for the pipeline; (3) the data acquisition and processing system was turned on to collect and record pressure changes; (4) the SAP slurry was injected into the pipeline through the injection device to photograph and record particle movement; (5) when the

Diagram 2 Water inrush simulation device for the karst pipeline

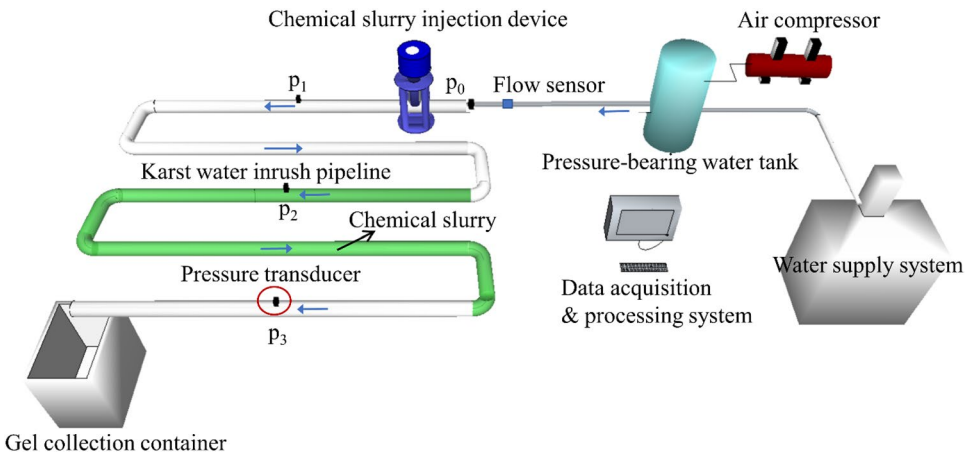

slurry diffused to the boundary of the water outlet or the flow was completely blocked by the gel, grouting was stopped; and (6) the images were analysed to determine the migration characteristics.

Results and Discussion

Analysis of Structural Characteristics of the SAP

The basic structural information for the SAP is provided in Fig. 1 and supplemental Figures S1 and S2. The FTIR spectra in Fig. 1a show that the − OH stretching vibration peak in the polymer structure occurs at 3,357 cm^{-1}, and the peak area is wide. In addition, the peak at 1,659 cm^{-1}

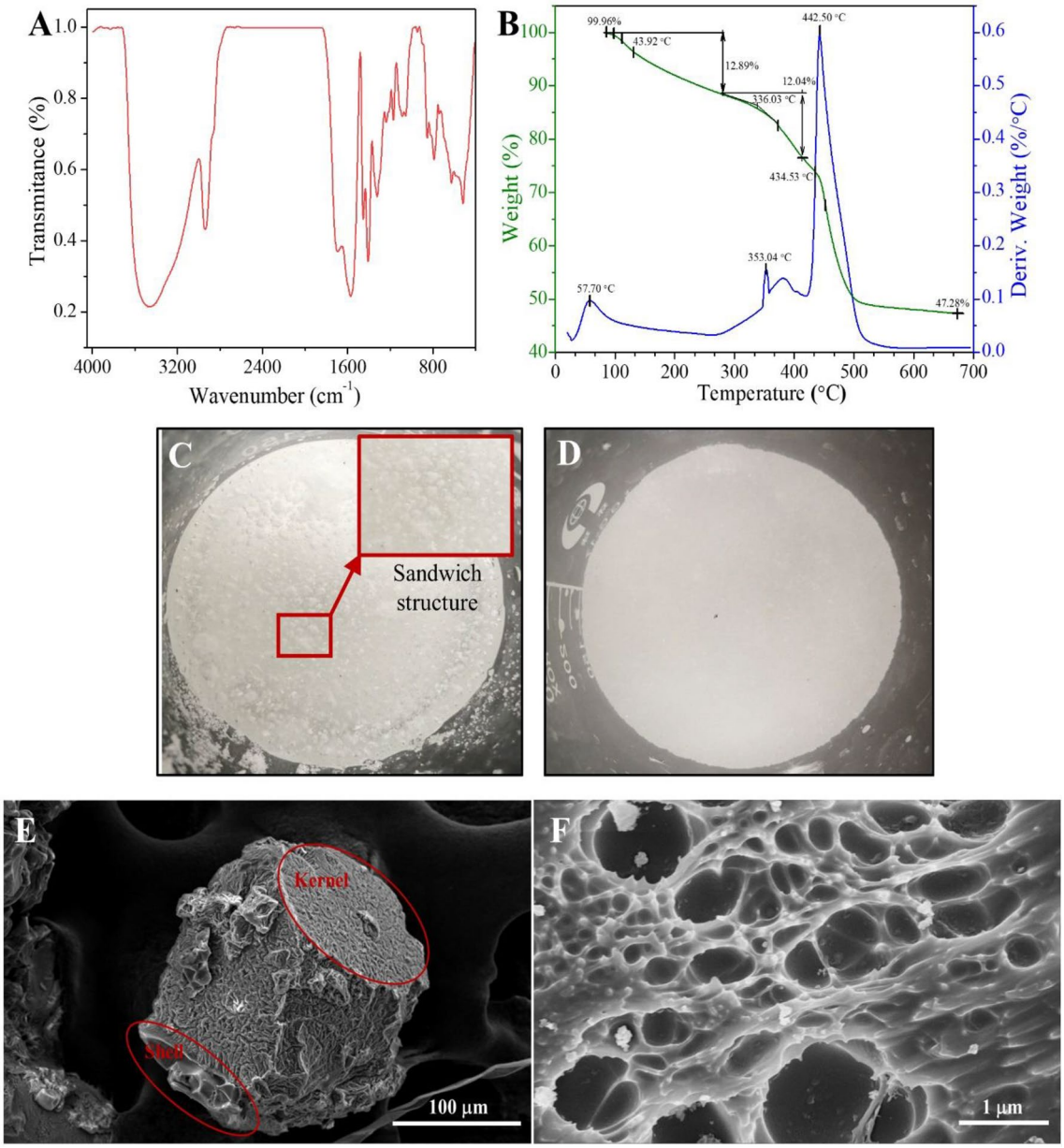

Fig. 1 FTIR spectra (**a**) and TGA diagram (**b**) of the obtained SAP. Water absorption state of the SAP before (**c**) and after (**d**) surface treatment (to facilitate the observation of the sandwich structure, no dye was added during the synthesis process). SEM images of the SAP before (**e**) and after (**f**) water absorbent. The samples for **a**, **b**, and **e** were used after drying while the samples for **d** were used after freeze-drying

corresponds to the stretching vibration of C=O and the observed peaks at 1,624 (strong peak) and 1470 cm^{-1} (medium peak) corresponds to a carboxylate radical in the polymers. Thus, one can conclude that the polymer contained many hydrophilic groups, demonstrating the outstanding water absorption ability of the SAP. The thermal stability analysis in Fig. 1b demonstrates three thermal weight loss events in the curve as the temperature increased from 20 to 700 °C, a mass loss of 12.39% from 18 to 278 °C, a small loss of approximately 5.78% from 278 to 434 °C, and a mass loss of 23.12% from 434 to 528 °C, which likely corresponded to the volatilization of free water in the SAP, the volatilization of bound water, and degradation of carboxylic acid groups in the SAP, and the degradation of polyacrylic acid and breakage of C–C single bonds, respectively. Therefore, we can deduce that the SAP can maintain very good thermal stability when facing water inrush from karst geology (generally below 40 °C).

The SAP without surface treatment had a very strong water absorption capacity. After contact with water, it easily formed a surface hydrogel layer, which prevented water molecules from entering the material and formed a sandwich state (Fig. 1c), significantly reducing the absorption capacity. To avoid this phenomenon and promote uniform absorption, the surface was modified (see support information 1 for the modification methods). Figure 1d shows the absorption effect after modification, where the surface gelation phenomenon is no longer observed. The SAP microstructures before and after water swelling were also revealed by SEM. As shown in Fig. 1e, the shape of the polymer is irregular, and includes massive edges and corners. There were also some incomplete shell-like structures that adhered to the surface.

The shell-like structure is related to the addition reaction of vinyl carbonate with polyacrylic acid at 150 °C; in contrast, the esterification reaction between glycerol and carboxylic acid groups occurs on the SAP surface. The shell structure formation increases the cross-linking density on the SAP surface. Therefore, the SAP forms a functional gradient material whose cross-linking density gradually decreases from the outside to the inside. Due to the shell structure adhering to the SAP surface, the water absorption velocity changes significantly. The beneficial effect is an increased SAP expansion velocity, which can meet the requirements of different geological conditions for material expansion performance. The experimental data are described in detail below. After water absorption, the SAP morphology changed from a core–shell structure to a fully extended three-dimensional network structure (Fig. 1f), indicating a good water swelling property and increased specific surface area, which was confirmed by the BET analysis (supplemental Fig. S2).

Water Absorption Capacity of the SAP

Water Absorption

The water absorption of the SAP significantly influences the effectiveness in plugging the gushing water; the greater the saturated water absorption quantity of the SAP, the more effective it is at filling rock fissures and plugging the inrush water. As shown in Fig. 2a, the SAP synthesized by this method had a water absorption rate of up to 321.2 times the initial rate. In addition, the particle size of the SAP had no effect on the ratio but had a significant effect on the water absorption velocity. To clarify this, a time-dependent curve of the water absorbance properties of the SAP with different particle sizes was drawn (Fig. 2b). The small particles expanded more rapidly than the large particles, which is attributed to the different specific surface areas. A large specific surface area exposes more hydrophilic groups, and thus increases the contact area between hydrophilic groups and water and the absorption rate. Interestingly, particles over 100 mesh in size required ≈ 3 min to reach the saturation state, even though they could reach 71% of the maximum absorption in the first 1.5 min. As a matter of comparison, 16–20 mesh SAP required ≈ 8 min to reach the highest absorbency. As shown in Fig. 2c, the curves show a decreasing trend after initially increasing, which directly reflects the SAP's water absorption process (Feng et al. 2014; Ge et al. 2006). Before water absorption, the polymer network is compact and the ions inside are not ionized into ion pairs. Once in contact with water, the water molecules combine with several hydrophilic groups on the SAP surface through hydrogen bonds, the hydrophilic groups begin to dissociate, the number of anions increases continuously, and the network begins to expand due to the electrostatic repulsion force between the anions (Lee et al. 2018; Ou et al. 2015). Meanwhile, the cation concentration inside the SAP increases, the osmotic pressure inside and outside the network increases, and more water molecules enter the SAP. With the increase in water absorption, the cation concentration in the SAP decreases, and the osmotic pressure difference between the inside and outside of the SAP approaches zero. When the elastic contraction force produced by the three-dimensional network structure expansion equals the anion electrostatic repulsion force, the water absorption reaches equilibrium (Farzanian and Ghahremaninezhad 2018; Li et al. 2009).

Based on the above experimental results, we inferred that particle size significantly influences the water absorption rate. Moreover, the absorption rate and the expansion velocity of the SAP can be adjusted by controlling the particle size distribution. This is consistent with the method used in practical engineering applications. In addition, an uneven particle distribution is conducive to particle interaction,

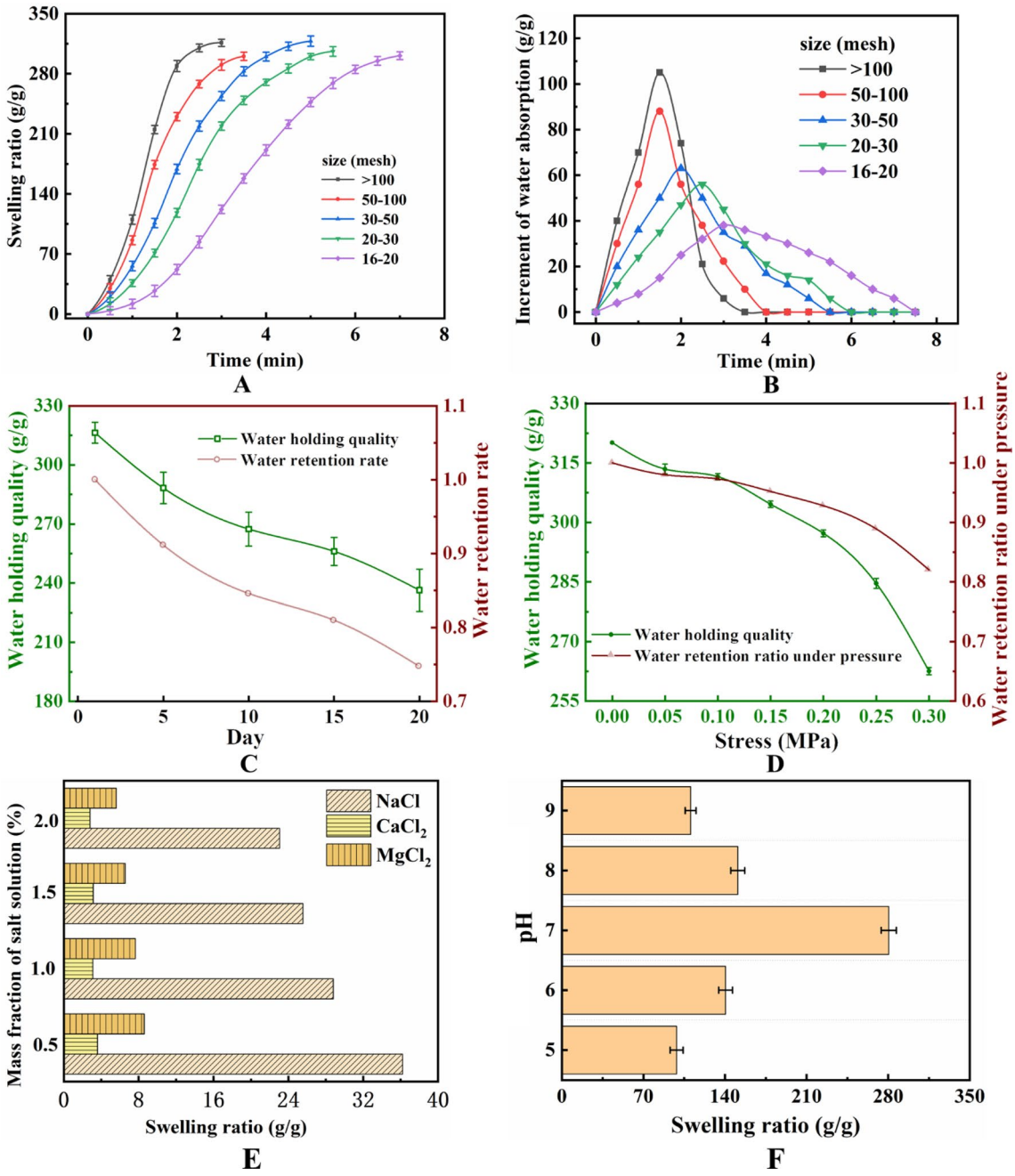

Fig. 2 **a** Swelling ratio curves, **b** water absorption rate curves of the SAP with different particle sizes, **c** water retention test curve under natural conditions, and **d** under pressure, **e** Effect of ion concentration on expansion performance, **f** Effect of pH on expansion performance

increasing the interaction probability and area between particles, which aids in the formation of a denser structure and achieves a better sealing effect.

Water quality has a significant influence on the expansibility of materials (Feng et al. 2014). Similarly, soil salinity is the key factor affecting water quality and soil salinity generally decreases with increasing soil depth (Zhao et al. 2016). In addition, there is a significant and strong power function relationship between surface-layer soil salinity and deep-layer soil salinity (Wang et al. 2018a, b, c). The ratio between the concentrations of different ions can also undergo important changes due to the adsorption and desorption of colloids in soils (Alvarez-Rogel et al. 1997). To study the influence of groundwater quality on water absorption, a complementary test was performed on the ion concentration and species (Fig. 2e). Different kinds of salts affect water absorption differently, with water absorption for the composites in salt solutions decreasing with increasing ion

concentration. Likewise, the water adsorption capacity of the SAP in different salt solutions follows an ascending order: $CaCl_2 < MgCl_2 < NaCl$, which is not difficult to explain when we carefully analyse each ion's information. Ca^{2+} and Mg^{2+} are in the same main group and have a larger ion radius and stronger coordination ability with the carboxyl group than Mg^{2+}. Mg^{2+} and Na^{+} are in the same period and have more valence electrons and stronger reactivity with carboxyl group. The pH also has a great influence on the expansion ratio. The expansion ratio of SAP is the highest at pH 7. With increasing or decreasing pH, the expansion ratio shows different degrees of loss (Fig. 2f). This undesired water absorbing-loss is caused by differences in osmotic pressure between the hydrogel's external and internal network. Several interpretations have been proposed (and validated) to explain this observation (Narayanan et al. 2018), including that the introduction of external ions shields the charge fixed on the polymer, thus reducing the electrostatic repulsive force, and finally reducing the water absorption of the resin. The experimental data in this part provides a basis for further research on karst pipe type water plugging in different areas.

Water Retention

As mentioned above, the SAP has dual properties of water absorption and water loss, with water loss negatively affecting plugging performance. It appears that after blocking the groundwater, the SAP located in the middle of the pipeline decreased in volume without a continuous water supply, which gradually reduced the expansion stress between the polymer particles, leading to a decreased the bearing capacity and instability in the temporary plugging body. Therefore, polymers with excellent water retention properties can provide relatively long-duration expansive stress to ensure the smooth operation of follow-up construction (reinforcement with cement slurry, for example). To evaluate the water retention performance of the polymer, two indices (natural water retention performance and pressurized water retention performance) were tested in the laboratory; the results are shown in Fig. 2d. Under natural conditions (room temperature, 30% humidity), the SAP maintained 75% water after 20 days, and the average water loss rate was ≈ 8% per week.

In addition, pressure can affect the polymer's water retention. The relationship between water retention and pressure (Fig. 2e) shows that the absorbed water is gradually lost with an increasing pressure. When a pressure of 0.3 MPa was applied for 1 min, the water retention rate decreased to 82%, due to the interaction of intramolecular valence bonds. The water molecules bind to hydrophilic groups through hydrogen bonds, such as carboxyl and hydroxyl groups, making it difficult for expansive resins to release water under pressure.

Simulation Experiment of Water Inrush Plugging

Selection of carrier fluid and SAP slurry configuration

As the SAP is granular, it can be injected into a karst pipeline and only draws support from the carrier fluid during the grouting process. In water inrush control, the SAP is mixed with the carrier fluid to form a slurry, which is then transported to the karst pipeline by a grouting pump. It can be difficult to choose an appropriate carrier fluid for the polymers, but since the water in the solution or carrier fluid is continuously absorbed once in contact with the SAP, water-containing solvents or solutions are inappropriate as carrier fluids for SAP transport. Indeed, the selection of the carrier fluid has become a key factor for successful SAP injection into karst areas. Combined with the nature of the material and grouting requirements, the carrier fluid must possess the following properties: (1) outstanding characteristics to suspend and carry particles; (2) good stability at high temperatures or pressures; (3) inert reactivity with the SAP under normal circumstances; (4) excellent miscibility with water; and most importantly, it must be (5) green, safe, and nontoxic to the environment. Based on the above requirements, glycerol and ethanol were selected as the SAP carrier fluids. Specifically, glycerol is a colourless and transparent liquid, is nontoxic for oral administration up to a certain concentration (3.15 g/kg), can be mixed with water at any ratio, does not react with SAP under normal conditions, and has a good carrying capacity (Chen, et al. 2012). However, glycerol has a relatively high viscosity (20 °C, 1,412 mPa·s; 25 °C, 945 mPa·s), and can interfere with the grouting process. Ethanol, also a colourless and transparent liquid, is nontoxic for oral administration at a certain concentration (7.06 g/kg), and has a very low viscosity (1.074 mPa·s, 20 °C); however, it has a poor carrying capacity (Kadlec et al. 2010). To obtain a carrying liquid with a strong carrying capacity and low viscosity, a mixture of glycerol and ethanol was used.

Qualitative Analysis of the Slurry Migration Mechanism in Karst Pipelines

The design of the water inrush plugging simulation equipment is shown in Fig. 3. At the beginning of the experiment, the slurry was configured and placed into the container for reserve. To effectively prove that the grouting material had a suitable water inrush sealing ability, the amount of grout used for this group of tests was less than in the other experiments; the total mass of the SAP was 200 g. As the expansion rate of the SAPs with a small particle size is quite rapid, only 50 g of SAP with a mesh larger than 100 was used to prevent plugging at the orifice. The use of an SAP with different particle diameters is conducive to the formation

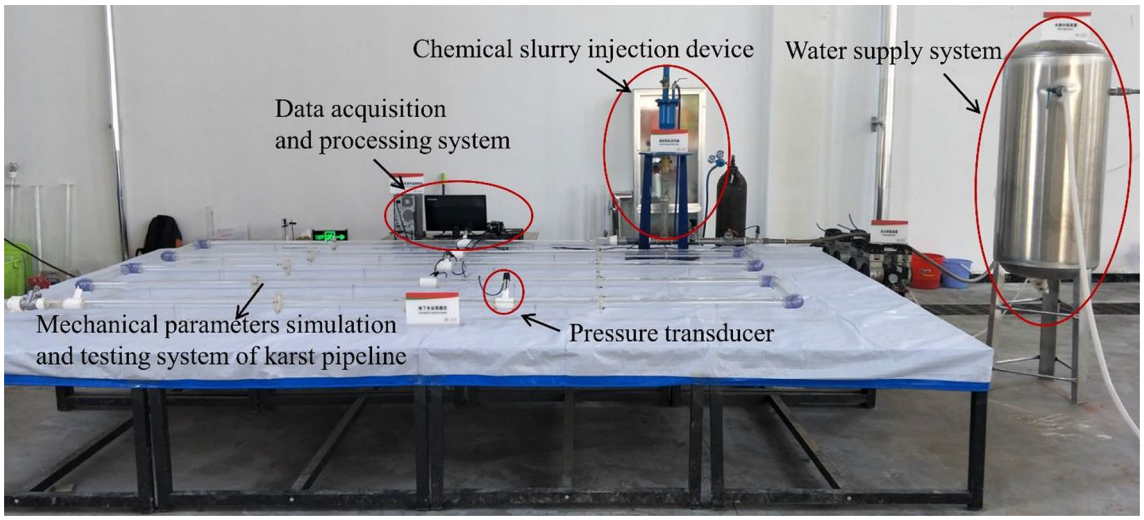

Fig. 3 Water inrush simulator for the karst pipeline

Table 3 Composition of the SAP slurry

Material	Mass (g)	
SAP	> 100 mesh	50
	> 50 & ≤ 100 mesh	100
	> 30 & ≤ 50 mesh	50
Carrier fluid	Glycerol	200
	Alcohol	100

The mud was prepared proportionally and placed into the feeder for standby

of a dense structure. Table 3 lists the specific ratio of SAP slurry, where SAP: glycerol: alcohol = 2:2:1. Several phases of our experiment are presented here. The system was operated with a 20 L/min constant flow for the pipeline through the water supply system. Subsequently, the data acquisition system was opened to monitor the pressure changes. Finally, slurry was injected into the pipeline, and the plugging effect was observed. For a clearer observation of the slurry movement in the water inrush pipeline, green dye was crosslinked into the SAP in the material synthesis stage. The grouting diffusion mechanism, water inrush plugging mechanism were analysed, and the plugging effect was evaluated using the already described visualization model,

The migration of the slurry, especially the SAP, in the pipeline can be clearly observed in Fig. 4a. The transport of mud and sand in rivers can be divided into traction (bed load) and suspended loads (Kim et al. 2018; Ma et al. 2017). Similarly, based on the movement of the SAP in the pipeline (Fig. 4), the polymer particles were divided into traction and suspended loads. The former refers to the particles rolling, moving, jumping, or moving along the bottom of the pipeline, while the latter refers to the small particles suspended in the water and moving from the bottom of the karst pipeline in a suspended manner under the influence of turbulence (Tokpohozin et al. 2015; Tsai et al. 2010). During the early stage of grouting, when the slurry was injected into the karst pipeline, the relative slurry density was similar to that of water, and the slurry moved in the form of a suspended load, as shown in Fig. 4b and Video 1. (The videos, along with the supplemental figures, were published along with the on-line version of this paper.) The trajectory of the suspended load in the flow was irregular, but its velocity in the flow direction was roughly the same as that of the water.

As the carrier fluid gradually dissolved in the water, the polymer particles were exposed, absorbed water, and expanded, gradually causing the suspended load to become bed load (Fig. 4c, d, Video 2). This occurred because the flow force acting on the SAP was greater than the cohesive force and the flow moment at the fulcrum of particles was greater than the cohesive moment (Fig. 4e). With the increase in the amount of traction load polymers, the potential and kinetic energies of the water flow was gradually consumed. Traction load particles constantly collide, leading to momentum exchange, and producing a discrete force vertical to the flow direction. The discrete force is transferred to the bottom of the pipeline through the interaction of particles, thus enhancing the compactness of the particles. With the water absorption and expansion of the polymer during migration, the particles squeeze each other and form a sealing body. Finally, water inrush sealing is realized by the wall friction force generated by the expansion force of the sealing body.

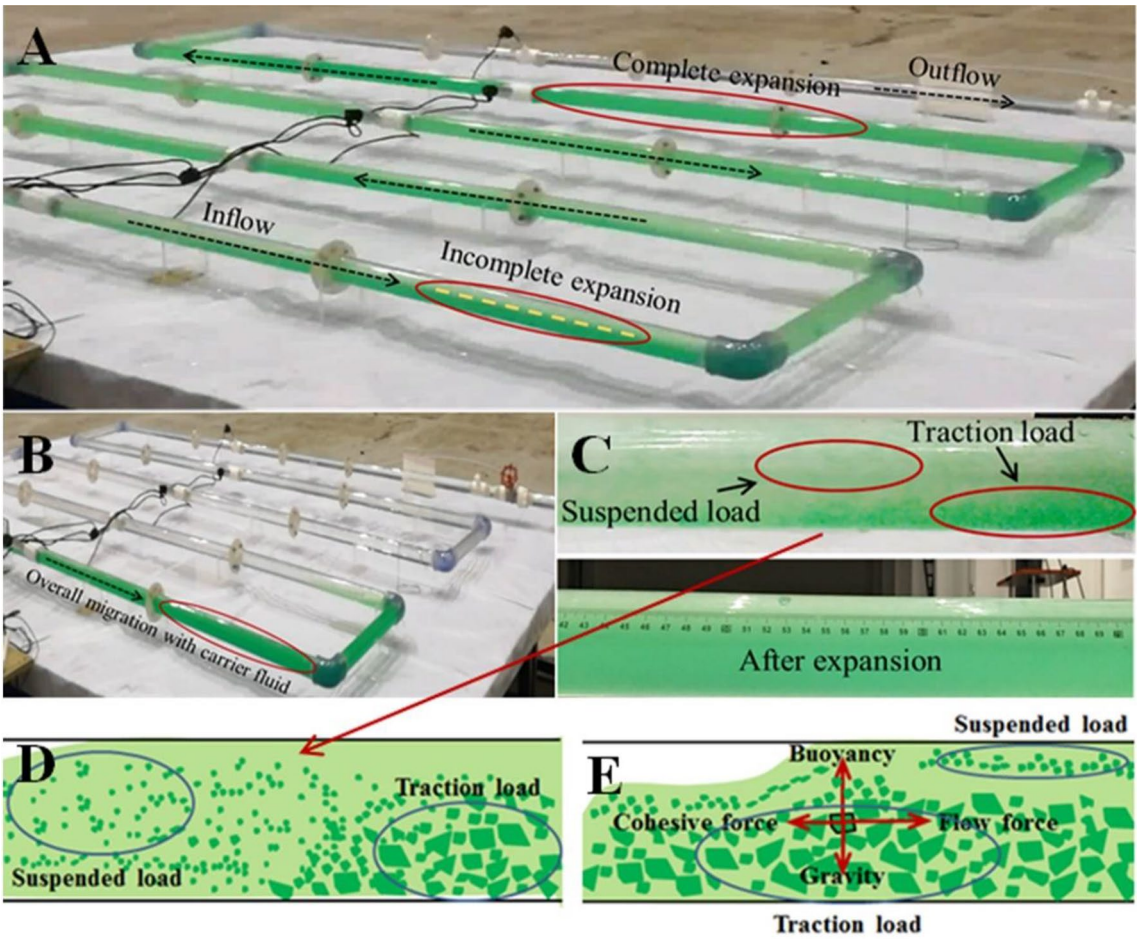

Fig. 4 **a** Slurry migration process; **b** overall migration of polymer particles with the liquid carrier; **c** transport and expansion compaction of the SAPs; **d** schematic diagram of the movement form of the polymer particles; and **e** analysis of the forces acting on the particles

Quantitative Analysis of Slurry Plugging Mechanism in Karst Pipeline

Figure 5a shows the time-dependent pressures at different pipeline locations. Initially, the water flow pressure gradually increased, but after ≈ 15 s, the monitoring curves at different positions all showed peak values. The pressure at P1 increased first, due to the opening of the slurry injection device, as the SAP slurry was pressed into the pipeline, and the flow pressure increased rapidly. The change in water pressure in Fig. 5b confirms this point. After the slurry was fully injected into the pipeline, the flow pressure gradually decreased and stabilized, as shown by a1, a2, and a3 in Fig. 5a. The duration of a1 was the longest, but the pressure was highest, which can be explained by the phenomenon described previously. Briefly, the SAP that entered the pipeline earliest spent the longest time in the pipeline and was the first SAP to continuously absorb water and expand. As the process of water flow and expansion continued, the pressure at P3 rose first. Figure 5b shows the slurry velocity change curve at P0, which directly reflects the change in the grouting pressure in the pipeline. The flow rate began to decrease 35 s after grouting, also indicating the beginning of the increase in grouting pressure, which is consistent with the results in Fig. 5c. As the grouting process and the absorption of water by the SAP continued, the volume of the SAP continued to expand. As a result, the piston section containing the SAP constantly increased. Eventually, the pressure and friction caused by SAP expansion could not be ignored. When the expansion stress rose to a certain degree, the pressure at P1, P2, and P3 stabilized (Fig. 5a). The time required for P1, P2, and P3 to reach the maximum pressure was 87, 80, and 70 s, and the maximum pressures were 1.5, 1.0, and 0.8 kPa, respectively. This phenomenon was controlled by either the SAP migration distance or the pipeline distance. Specifically, the distance between P3 and P0 was larger than that between P2 and P0 and P1 to P0, such that the SAP particles that migrated to P3 expanded more fully than those at P2 and P1. Due to the pipeline limitation, the pipeline at P3 was first blocked from reaching

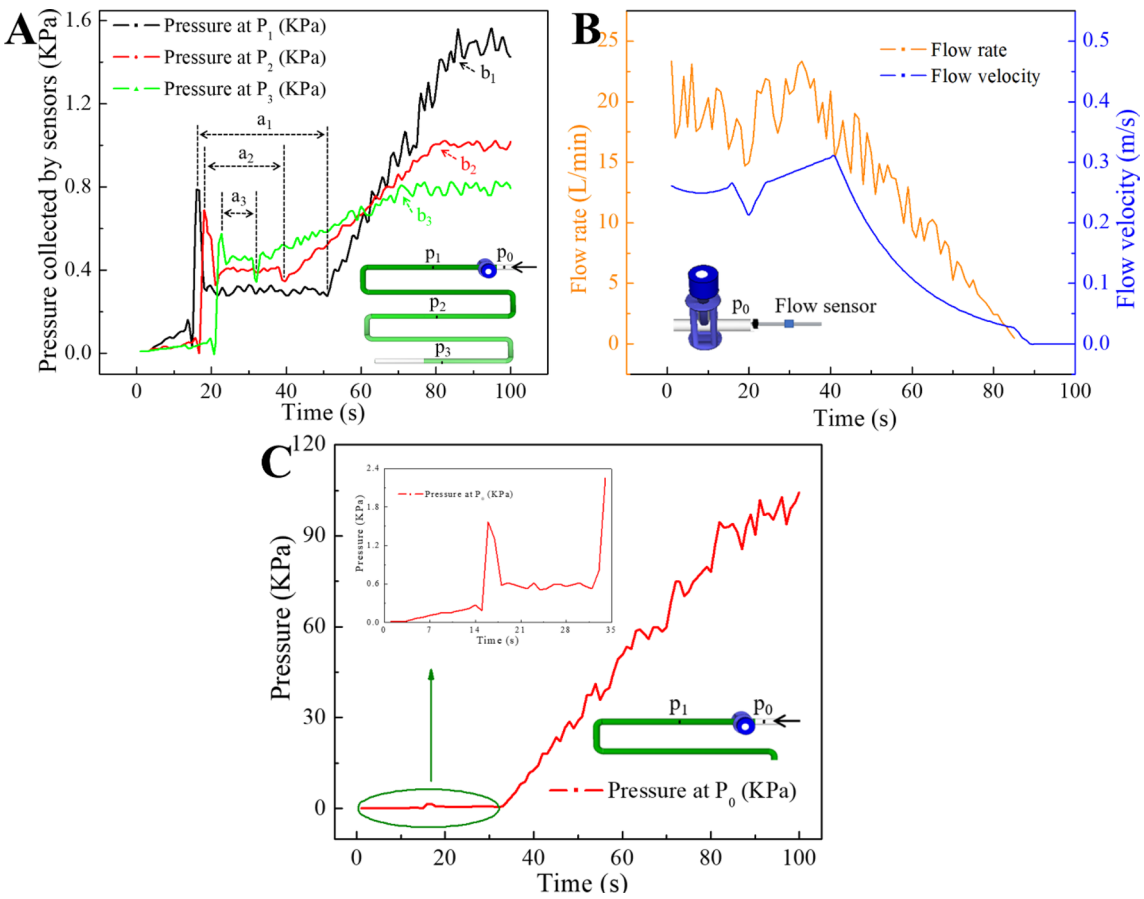

Fig. 5 **a** Pressure monitoring curves at different locations; **b** water flow monitoring curve at P0; and **c** water pressure monitoring curve at P0

the maximum pressure. With continued grouting, the SAP particles migrated to P3 and formed an adjacent sealing piston. This action caused an early pipeline water flow fault, and the pressure caused by the water flow was discharged. However, the piston expansion counteracted the impact pressure of part of the water flow. Therefore, the pressure at P3 first reached the maximum value, and the maximum value was the least among the three. In contrast, P1 was always under water flow pressure, and its value increased with time, reaching its maximum after the water inrush was completely blocked. The experimental results are also consistent with the flow rate change at P0 in Fig. 5b, in which the water flow rate was initially constant and then decreased continuously during grouting and plugging. Finally, the flow rate was 0 and stable. To understand the process more intuitively, a video of the blocked water inrush is provided in the supporting information (Video 3).

Through the above simulation experiment on karst pipeline water inrush blocking, we prove that the SAP slurry effectively plugged the water inrush. Moreover, contrary to expectation, the water inrush (flow rate of 20 L/min and flow velocity of 0.3 m/s) was plugged by only 500 g of SAP slurry. Compared with traditional slurry, the SAP material has notable advantages in the karst conduit water inrush treatment, including a high expansion ratio, relatively low dosage, and excellent plugging effect.

Treatment Strategy for Water Inrush

The SAP slurry was configured to transform from dynamic to static karst water inflow. Then, a common cement slurry was injected after the plugging body. During water inrush plugging, the large polymer swells and extrudes, gradually forming a skeleton structure. Ultimately, polymers with different particle sizes accumulate in the skeleton structure and continue to swell, presenting a dense skeleton structure, which temporarily plugs water inrush. After the flow velocity decreases or stops surging, the cement slurry was injected. The plugging body formed by the polymer guarantees cement slurry retention; furthermore, the subsequent cement slurry supplements the strength of the temporary plugging body. Consequently, both the strength of the temporary plugging body and the stability of the surrounding rock are improved, and the problem of cement slurry

retention under dynamic water flow is also solved. These results provide new insights for the treatment of karst water inrush grouting in tunnels; Video 4 and Diagram S1 provide a more intuitive illustration.

Application Prospects and Environmental Benefit Analysis of SAP Water Inrush Plugging

With the rapid development of urbanization, the use of underground space is developing rapidly worldwide, and underground engineering accidents occur frequently. Water inrush disasters caused by the construction of underground space in karst areas rank first among such accidents. The demand for water inrush disaster management is gradually appearing in the broad market. Innovative and breakthrough materials for disaster prevention and control can help to solve the technical problems associated with governance, conform to the substantial demand for infrastructure construction for water inrush disaster management, and have broad application prospects.

In view of the characteristics of the fast flow rate and large flow of water inrushes in karst areas, this study proposes the treatment of water inrush by SAP, which will have a beneficial effect on the environment. First, SAP is an effective treatment for water inrush in karst areas, prevents ground collapse and other geological disasters caused by water disasters underground, and eliminates casualties and economic losses caused by water inrush. Second, given the large water flow in karst areas, drainage technology is often implemented before grouting, which can cause the water level in the surrounding area to drop and the ground stress to change, resulting in uneven settlement of foundations and cracks, adversely affecting the service life of the surrounding buildings. Such drainage can easily disrupt the groundwater circulation system and the original groundwater balance and damage the ecological environment. The treatment method proposed in this study can block water inrush in karst areas without drainage and speed reductions; therefore, SAP grouting material has potential application value in the field of underground engineering, with significant social benefits.

Conclusion

In summary, this study demonstrates an effective sealing material for the treatment of water inrush. In addition, it provides a method for synthesizing SAPs with an expansion ratio as high as 321.2, a shell structure, and good thermal stability. To evaluate the plugging effect of the SAP, a water inrush simulation device was designed. Unexpectedly, with only 200 g of SAP, the pipeline water flow (20 L/min, 0.3 m/s) was completely blocked in a few minutes and the real-time process of water inrush plugging was clearly recorded. The mechanism of water inrush plugging and rules for SAP migration were expounded. We plan to optimize this technology and perform field tests in a follow-up study. This research may contribute to controlling the occurrence of major water inrush disasters in karst areas, thereby safeguarding humans and property, as well as protecting the ecological environment.

Supplementary Information The online version contains supplementary material available at https://doi.org/10.1007/s10230-021-00802-1.

Acknowledgements The authors are grateful for the financial support from the National Key Research and Development Project (2019YFC1805402), Basic scientific research business expenses of Shandong University (31560079614116), Natural Science Foundation of Shandong Province of China (Grant ZR2020QE262 & ZR2020QE291), and the Young Elite Scientists Sponsorship Program by CAST (2018QNRC001).

References

Abdulbaki M, Huh C, Sepehrnoori K, Delshad M, Varavei A (2014) A critical review on use of polymer microgels for conformance control purposes. J Petrol Sci Eng 122:741–753

Alvarez-Rogel J, Hernandez J, Silla RO, Alcaraz F (1997) Patterns of spatial and temporal variations in soil salinity: Example of a salt marsh in a semiarid climate. Arid Soil Res Rehab 11:315–329

Cao M, Wang C, Xia R, Chen P, Miao J, Yang B, Qian J, Tang Y (2018) Preparation and performance of the modified high-strength/high-modulus polyvinyl alcohol fibre/polyurethane grouting materials. Constr Build Mater 168:482–489

Chen C, Li W, Song Y, Weng L, Zhang N (2012) Effects of glycerol concentrations on self-diffusion coefficients of glycerol in glycerol-water-sodium chloride ternary solutions. Acta Chim Sinica 70(8):1043–1046

Chen Z, Dong M, Husein M, Bryant S (2018) Effects of oil viscosity on the plugging performance of oil-in-water emulsion in porous media. Ind Eng Chem Res 57(21):7301–7309

Cui W, Huang J, Song H, Xiao M (2017) Development of two new anti-washout grouting materials using multi-way ANOVA in conjunction with grey relational analysis. Constr Build Mater 156:184–198

Cui C, Guo C, Wang F (2019) Fatigue analysis for void repair of cement concrete pavement with under slab by polymer grouting. Civ Eng J-Tehran 5(7):1452–1464

Duan B, Li L (2012) Grouting reinforcement technique for subsurface excavation of group metro tunnels construction in complex environment. Disaster Adv 5(4):1508–1512

Fan H, Zhang Y, He S, Wang K, Wang X, Wang H (2018) Hazards and treatment of karst tunneling in Qinling-Daba mountainous area: overview and lessons learnt from Yichang-Wanzhou railway system. Environ Earth Sci 77(67919)

Farzanian K, Ghahremaninezhad A (2018) Desorption of superabsorbent hydrogels with varied chemical compositions in cementitious materials. Mater Struct 51(UNSP 31)

Feng D, Bai B, Ding C, Wang H, Suo Y (2014) Synthesis and swelling behaviors of yeast-g-poly(acrylic acid) superabsorbent co-polymer. Ind Eng Chem Res 53(32):12760–12769

Ge H, Pang W, Luo D (2006) Graft copolymerization of chitosan with acrylic acid under microwave irradiation and its water absorbency. Carbohyd Polym 66(3):372–378

Guo MY, Liu MZ, Zhan FL, Wu L (2005) Preparation and properties of a slow-release membrane-encapsulated urea fertilizer with superabsorbent and moisture preservation. Ind Eng Chem Res 44(12):4206–4211

Jia H, Pu W, Zhao J, Jin F (2010) Research on the gelation performance of low toxic PEI cross-linking PHPAM Gel systems as water shutoff agents in low temperature reservoirs. Ind Eng Chem Res 49(20):9618–9624

Kadlec P, Henke S, Bubnik Z (2010) Properties of ethanol and ethanol-water solutions - tables and equations. Zuckerindustrie 135(10):607–613

Kim D, Kim B, Choi B (2018) Adaptability of suspended sediment transport model for sandbar migration simulation. J Coastal Res 85:661–665

Lee S, Moon BJ, Lee HJ, Bae S, Kim T, Jung YC, Park JH, Lee SH (2018) Enhancement of adsorption performance for organic molecules by combined effect of intermolecular interaction and morphology in porous rGO-incorporated hydrogels. ACS Appl Mater Inter 10(20):17335–17344

Li Y, Xu T, Ouyang Z, Lin X, Liu H, Hao Z, Yang P (2009) Micromorphology of macromolecular superabsorbent polymer and its fractal characteristics. J Appl Polym Sci 113(6):3510–3519

Liu Y, Dai C, Wang K, Zhao M, Gao M, Yang Z, Fang J, Wu Y (2016) Investigation on preparation and profile control mechanisms of the dispersed particle gels (DPG) formed from phenol formaldehyde cross-linked polymer gel. Ind Eng Chem Res 55(22):6284–6292

Ma D, Duan H, Li X (2019a) Effects of seepage-induced erosion on nonlinear hydraulic properties of broken red sandstones. Tunn Undergr Sp Tech 91:102993. https://doi.org/10.1016/j.tust.2019.102993

Ma D, Duan H, Liu J (2019b) The role of gangue on the mitigation of mining-induced hazards and environmental pollution: An experimental investigation. Sci Total Environ 664:436–448. https://doi.org/10.1016/j.scitotenv.2019.02.059

Ma D, Duan H, Liu W (2020) Water–sediment two-phase flow inrush hazard in rock fractures of overburden strata during coal mining. Mine Water Environ 39(2):308–319. https://doi.org/10.1007/s10230-020-00687-6

Ma H, Nittrouer JA, Naito K, Fu X, Zhang Y, Moodie AJ, Wang Y, Wu B, Parker G (2017) The exceptional sediment load of fine-grained dispersal systems: example of the Yellow River, China. Sci Adv 3(16031145). doi: https://doi.org/10.1126/sciadv.1603114

Ma D, Cai X, Li Q, Duan H (2018) In-situ and numerical investigation of groundwater inrush hazard from grouted karst collapse pillar in longwall mining. Water-Sui 10(9). doi:https://doi.org/10.3390/w10091187

Narayanan A, Kartik R, Sangeetha E, Dhamodharan R (2018) Super water absorbing polymeric gel from chitosan, citric acid and urea: Synthesis and mechanism of water absorption. Carbohyd Polym 191:152–160. https://doi.org/10.1016/j.carbpol.2018.03.028

Ni B, Lu S, Liu M (2012) Novel multinutrient fertilizer and its effect on slow release, water holding, and soil amending. Ind Eng Chem Res 51(40):12993–13000

Ou X, Han Q, Dai H, Wang J (2015) Molecular dynamic simulations of the water absorbency of hydrogels. J mol model 21(2319)

Shamsuddoha M, Huesken G, Schmidt W, Kuehne H, Baessler M (2018) Ternary mix design of grout material for structural repair using statistical tools. Constr Build Mater 189:170–180

Sun L, Han Q, Li D, Zhang X, Pu W, Tang X, Zhang Y, Bai B (2019) Water plugging performance of preformed particle gel in partially filled fractures. Ind Eng Chem Res 58(16):6778–6784

Tokpohozin NB, Kounouhewa B, Avossevou GYH, Houekpoheham A, Awanou CN (2015) Modelling of sediment movement in the surf and swash zones. Acta Oceanol Sin 34(2):137–142

Tsai C, Tsai C, Weng C, Bair J, Chen C (2010) Calculation of bed load based on the measured data of suspended load. Paddy Water Environ 8(4):371–384

Wang Q, Zhu Q, Shao T, Yu X, Xu S, Zhang J, Kong Q (2018a) The rheological test and application research of glass fibre cement slurry based on plugging mechanism of dynamic water grouting. Constr Build Mater 189:119–130

Wang Y, Deng C, Liu Y, Niu Z, Li Y (2018c) Identifying change in spatial accumulation of soil salinity in an inland river watershed, China. Sci Total Environ 621:177–185. https://doi.org/10.1016/j.scitotenv.2017.11.222

Wang X, Yao J, Li X, Guo Y, Shen A, Pu H (2018) Mechanical properties improvement mechanism of silica fume-modified ultrafine cement used to repair pavement microcracks. Adv Mater Sci Eng (4898230). doi: https://doi.org/10.1155/2018/4898230

Yao C, Wang D, Wang J, Hou J, Lei G, Steenhuis TS (2017) Effect of ionic strength on the transport and retention of polyacrylamide microspheres in reservoir water shutoff treatment. Ind Eng Chem Res 56(28):8158–8168

Yuan C, Pu W, Jin F, Zhang Y, Jia H, Zhao T (2014) Performance of oil-based cement slurry as a selective water-plugging agent in high-temperature and high-salinity cave-fractured carbonate reservoirs. Ind Eng Chem Res 53(14):6137–6149

Yuan J, Chen W, Tan X, Yang D, Zhang Q (2020) New method to evaluate antiwashout performance of grout for preventing water-inrush disasters. Int J Geomech 20(060190212)

Zhang C, Fu J, Yang J, Ou X, Ye X, Zhang Y (2018a) Formulation and performance of grouting materials for underwater shield tunnel construction in karst ground. Constr Build Mater 187:327–338

Zhang G, Jiao Y, Ma C, Wang H, Chen L, Tang Z (2018b) Alteration characteristics of granite contact zone and treatment measures for inrush hazards during tunnel construction—a case study. Eng Geol 235:64–80

Zhao Y, Feng Q, Yang H (2016) Soil salinity distribution and its relationship with soil particle size in the lower reaches of Heihe River, northwestern China. Environ Earth Sci 75. doi https://doi.org/10.1007/s12665-016-5603-8

Zhu D, Bai B, Hou J (2017) Polymer gel systems for water management in high-temperature petroleum reservoirs: a chemical review. Energ Fuel 31(12):13063–13087